

# Capillary flow and mechanical buckling in a growing annular bacterial colony

Tieyan Si<sup>1,2</sup>, Zidong Ma<sup>2</sup>, Jay X. Tang<sup>\*,2</sup>

<sup>1</sup>Harbin Institute of Technology, Harbin, China

<sup>2</sup>Brown University, Providence, Rhode Island, United States

\* Corresponding author: [jay\\_tang@brown.edu](mailto:jay_tang@brown.edu)

## Abstract

A growing bacterial colony is a dense suspension of an increasing number of cells capable of individual as well as collective motion. Starting by inoculating *Pseudomonas aeruginosa* over an annular area on an agar plate, we observe the growth and spread of the bacterial population, and model the process by consideration of physical effects that account for the features observed. Over a course of 10-12 hours, the majority of bacteria have migrated to and accumulated at the edges. We model the capillary flow induced by imbalanced evaporation flux as the cause for the accumulation, much like for the well-known coffee stain phenomenon. In the meantime, periodic buckles, or protrusions, occur at the inner edge. These buckles indicate that the crowding bacteria produce a jam, transforming the densely packed population at the inner edge to a solid state. The continued bacterial growth produces the buckles. Subsequently, a ring of packed bacteria behind the inner edge detaches from it and breaks into pieces, forming bacterial droplets. These droplets slowly coalesce while they continually grow and collectively surf on the agar surface in the region where the colony has previously spread over. We conclude that fluid dynamics and elasto-mechanics together govern the bacterial colony pattern evolution. This study offers a clear example that physical effects account for large scale patterns that develop in growing bacterial colonies.

## Introduction

Many species of bacteria thrive at a moist surface with nutrients supplied via a porous substrate such as an agar gel. These bacteria produce osmolytes, which draw nutrients containing fluid out of the substrate to fuel the growth of the bacterial population. They also secrete surfactants, which reduce surface tension at the air-liquid interface so that the bacteria containing fluid can spread over the agar surface. A large number of studies have been performed based on observing bacterial colony growth and spread. For example, starting from spot inoculation on an agar surface, various patterns can form, such as bullseyes [1, 2], dendrites [2], fractals like structures [1, 3], and so on.

The ability to be individually motile is an important property of most species of bacteria. The majority of motile bacteria are propelled by their flagella. However, bacterial motility can also be achieved by alternative mechanisms. For example, besides the flagellated motion commonly referred to as swimming, *Pseudomonas aeruginosa* can also slide over a solid surface by contraction of its Type IV pili [4-6]. Multiple bacterial genera, such as *Bacillus*, *Pseudomonas*, *Salmonella*, *Serratia*, and *Vibrio* [7], can spread rapidly under favorable conditions over a solid surface through collective motion, via a phenomenon called swarming. *Myxococcus xanthus* can swarm by extrusion of secretion [8, 9]. In some cases, bacterial spread may involve chemo-attractants and/or quorum sensors [2], but spreading can also be achieved through purely physical mechanisms, involving osmotic swelling [10, 11], surface forces [12], and fluid flow facilitated by capillary effect or even gravity [13]. These physical mechanisms of bacterial spreading do not require individual motility. They may account for the swarming motility of non-motile mutants of *Bacillus subtilis* [14], *Paenibacillus dendritiformis* [3], and *Pseudomonas aeruginosa* [15], for example.

There has been extensive research on mechanisms underlying bacterial swarming on an agar surface. Genetic regulation occurs in some species under certain environments to increase the number of flagella, so that the swarming speed increases [16, 17]. Biochemical mechanisms such as chemotaxis [1] and quorum sensing [18, 19] may trigger swarm dynamics in response to environmental changes. Models have been developed based on coupled reaction-diffusion equations for the spatial distribution of chemical agents and the cell density profile,

which can predict dendritic patterns as well as fractals similar to observed patterns [1, 20-22]. However, a recent experiment shows that the swarming motility of *P. aeruginosa* remains fast even in the absence of concurrent diffusion of nutrients over the surface by placing a physical barrier between two halves of agar [23]. Fauvart *et al.* [23] propose that the Marangoni flow induced by a surface tension gradient might drive the swarming of *P. aeruginosa*. We recently examined the influence of physical effects such as surface tension and gel permeability on the swarming motility of *P. aeruginosa* [24]. Our findings, consistent with several recent studies on *Bacillus subtilis* [13, 14, 25], show that swarming is restricted by the surface tension and contact line at the swarm front and the colony growth is limited by the rate of water supply from the agar substrate. Taken together, a general picture has emerged from numerous studies indicating that, while sensitively dependent on various parameters, swarming is a robust phenomenon and it can occur among diverse species of bacteria with different modes of individual motility.

We choose to work on *P. aeruginosa* as a model system to explore for effects of physical factors on bacterial colony expansion. *P. aeruginosa* is a strong swarmer. It expands on agar surfaces, forming a rich variety of patterns dependent on the strains used [26-29], amounts of rhamnolipids expressed (or added) [15, 30-32], as well as experimental conditions such as agar concentration [24], ambient humidity, and growth temperature [24, 33]. Besides swimming [34], swarming [23, 26, 32], and twitching motility [4, 35], *P. aeruginosa* also secrete extracellular matrix molecules, forming biofilms [35, 36]. Bacteria within biofilms can sustain water loss, remain viable, and in some cases become antibiotic resistant [16, 37]. Since *P. aeruginosa* is a human pathogen that causes opportunistic infections in situations such as in open wounds, on medical implants, on respiratory tracts, etc., the study of growth and spread of *P. aeruginosa* at or near solid surfaces is of medical relevance.

In this report, we observe and study the colony growth and pattern evolution of *P. aeruginosa* under a specially designed geometry, an annular inoculation. Using this simple geometry, we show that the growing bacterial colony of *P. aeruginosa* displays properties of both a viscous fluid and an elastic solid. We explain our observation by applying physics concepts

including evaporation, capillary flow, colloidal jamming, elastic buckling instability, and Rayleigh–Plateau instability. We provide theoretical analysis of the observed phenomena, gaining insights on physical mechanisms that dictate the patterns formed by the growing bacterial population. Understanding these mechanisms may lead to development of useful strategies to control, facilitate, or inhibit the spread of microbes on various surfaces as needed.

## **Results and Discussion**

### ***Observation and initial assessment***

An annular bacterial colony inoculated on an agar plate undergoes several steps of pattern evolution. Fig. 1 shows a set of photos recording colony growth in different stages: homogeneous growth, accumulation of bacteria at the edges to form inner and outer rings, buckling at the inner edge to form periodic protrusions, breaking of the inner ring into droplets, migration of the droplets away from the inner edge, and fusion of the separate droplets back into a bolder ring. These complex dynamics are observed within the first 24 hours of growth. Over the next two days, the annular colony expanded further but gradually dried, appearing flower-shaped and leaving a vacant hole in the central region.

As a bacterial colony expands on an agar surface, it draws the nutrient-containing liquid out of the gel [10-12, 24]. The petri dish containing bacteria on the gel surface is covered but not sealed, allowing gradual evaporation, which reduces the fluid content of the growing colony. In the meantime, the surface tension, including the contact line pinning force at the edges [12], restricts the areal growth of the swarm in order to minimize the total surface energy. The competition between the surface tension and the internal pressure exerted by the growing bacterial population determines the expansion of the bacterial colony. The sequential photos during the first 6-15 hours of growth show that the majority of bacteria migrated to the inner and outer edges, nearly evacuating the inner area (Fig. 1). The bacterial density was measured based on the local brightness and the results are shown in a line plot (Fig. 2a), along with a close comparison between one point of the outer edge and a neighboring point in the

inner area (Fig. 2b). Previous work has shown that the intensity profile has a shape similar to the height profile of the bacterial colony, measured by white light interferometry [23]. Our observation and measurement following annular inoculation, as described above, confirm that most bacteria gradually migrate to the edges over time.

Conventional models on bacterial spreading on an agar surface, typically based on reaction-diffusion mechanism [1, 20] and chemotaxis [1, 22], cannot account for the features we have observed. According to the reaction-diffusion model, bacteria are expected to first consume the nutrients inland and then migrate outward to find more nutrients. This model would not predict a back flow of bacteria inward, either individually or in collective mass. We observed, however, that after attaining high cell density on the inner edge, a large fraction of bacteria migrated back in large droplets to the inland area (Fig. 1, 14-17 hrs). A fraction of bacteria on the outer edge also migrated back inward, albeit more gradually (Fig. 1, 15-21 hrs). This observation contradicts the reaction-diffusion model, which offers no mechanism for backward migration. We also cannot explain this observation based on another conventional model, namely, chemotaxis [1, 22]. It is unlikely, for instance, that a specific chemical attractant would drive the dense packs of bacteria to leave the edges and return to the inland where the same population of bacteria swept over previously.

### ***Edge accumulation due to evaporation and capillary flow***

We propose a fluid dynamic model to account for the experimental observation of edge accumulation. In this model, water evaporation acts as a counter-acting factor while the bacterial colony grows and expands. Capillary flow and inhomogeneous evaporation due to curvature variation cause the bacterial population to concentrate on the edges. A bacterial colony is in essence a dense suspension of motile cells in nutrient solution. The evaporation flux on the surface of this hybrid liquid varies with local curvature, with faster evaporation flux at locations of convex curvature [38, 39]. The evaporation flux  $J(x)$  on a spherical cap of liquid droplet can be quantified by the following equation [38],

$$J(x) = J_0 \left[ 1 - \left( \frac{x}{R} \right)^2 \right]^{-(1/2 - a/\pi)} . \quad (1)$$

Here  $x$  is the distance to the symmetry axis of the spherical cap,  $R$  is the spherical radius,  $a$  is the angle between the cap and the flat base, and  $J_0$  is the rate of evaporation at the tip of the cap, where  $x = 0$ . For a thin cap, most relevant to a thin layer of swarm fluid, the angle  $a$  is less than  $\pi/2$ , or  $90^\circ$ . The evaporation flux increases with local curvature. The surface of the bacterial colony near the edges is more convex than on the inner area. The higher evaporation rate on the edges induces a net capillary flow from the inner area to the edges, carrying bacteria in the fluid with it (Fig. 2d). Fig. 2c shows the flow field distribution on the radial cross-section of the bacterial annulus computed with a boundary condition set by the evaporation-flux equation. The increasing density of bacteria, due both to growth and to the influx of nearby cells towards the edges, causes them to eventually pile up there, further increasing the cross-sectional curvature on the edges. This pileup further increases the evaporation flux on the edges (Fig. 2d). In essence, the observed phenomenon is akin to the well-known coffee ring effect [38, 40, 41], which implies that individual bacterial motility is not even required for the edge accumulation effects.

The increasing cell density at the inner edge leads to the occurrence of a wavy coastal line with numerous small buckles not observed at the outer edge. The buckles become visible to the naked eye about 6 hours following inoculation. Fig. 3 shows fully developed buckles in 9 hours. The buckles are approximately periodic (Fig. 3b). The average wavelength of the buckles is  $2.5 \pm 0.2$  mm, measured for  $\sim 30$  buckles over the inner circumference. These buckles formed at the inner edge appear corrugated, with sharp grooves between neighboring protrusions. They do not match the smooth wavy edge of a perturbed liquid torus [42]. Instead, they are likely caused by mechanical deformation in order to release the internal stress of the front layer. Therefore, the buckling phenomenon in our bacterial swarm suggests that the inner edge has become a solid-like material.

The expansion of a growing bacterial colony is restricted at its edge by pinning of the contact line, a commonly occurring behavior of a partially wetting liquid film [43-45]. The radial

flow and evaporation cause the accumulation of bacteria on the edges. With increasing density, the bacteria at the edges exert increasing pressure on each other. They eventually reach the jamming threshold at the inner edge, transforming the region from a viscous fluid into a solid-like material [46]. As the population keeps growing, the internal stress at the inner edge gradually reaches a critical value at which point surface tension can no longer maintain the shape of a flat front. Instead, the inner edge deforms to release the internal stress and forms many buckles. Note that this stress-release model may not be applicable to the outer edge, as the circumferential length increases with the radius. With the same initial density, the inner edge is expected to attain higher density than that on the outer edge over time.

### *Analysis of buckling instability at the inner edge*

Many biological tissues grow periodic buckles [47], such as the inner surface of small intestines, blood vessels [48], and tumors [49]. These biological tissues have been modeled as growing hyper-elastic tubes [47, 50]. The buckling theory predicts that regularly distributed buckles can occur in hyper-elastic tubes. The model predicts both the onset of buckling and the number of buckles, which varies in animal tissues as a function of external pressure, growth rate and thickness of the tissue layer. An annulus of surfactant-containing water droplets can also display fingering protrusions [51], which is similar to the buckles here. A close comparison, however, reveals a key difference: The buckles we observe on the inner edge have sharp, inward grooves, whereas the fingering protrusions of water droplets show a smooth edge of inward arc. Therefore, hydrodynamic model cannot account for the buckles we observe.

We now apply the familiar Euler buckling model to make a crude estimate of a critical circumferential pressure required to account for the buckles observed. A short arc of the solid front is approximated by a straight, thin rod. The critical circumferential pressure (stress) of buckling mode  $n$  is

$$P(n) = \frac{n^2 \pi^2 EI}{L^2 A} \quad (2)$$

where  $L/n \approx 0.4$  cm is the length of the arc we typically observed. It is also the length of a buckle, which obeys the relation  $L/n = \lambda/2$ , where  $\lambda$  is the wavelength of the buckle.  $E$  is the Young's modulus. As a crude approximation, we take the Young's modulus of reported value for biofilms of *P. aeruginosa*,  $E \approx 1$  kPa [36].  $I$  is the 2<sup>nd</sup> or area moment of inertia. We treat the dense edges as a solid ring with circular cross section of radius  $r$ . Thus, the cross-sectional area is  $A = \pi r^2$ , and the area moment is  $I = \pi r^4/4$ . As a crude estimate and assuming circular cross-sections, we use  $r \approx 1$  mm, which is approximately the width of the inner ring. Plugging these parameters into Eq. (2) yields a critical stress  $P_{cr} \approx 154$  Pa (or  $154 \text{ N}\cdot\text{m}^{-2}$ ). This is the estimated threshold stress required for the buckles to occur.

We apply next the mechanical buckling model for a growing elastic tube [47, 50] to yield quantitative predictions. The small and periodic buckles only occur on the inner edge of the bacterial annulus. They are not found on the outer edge of the annulus. We assume that a thin front layer of the inner edge ring has the same physical property as an elastic tube. The inner and outer radii of the thin elastic layer (Fig. 3i) are denoted as  $R_{in}$  and  $R_{out}$ , respectively. The initial position of an arbitrary point on the inner edge of the annulus is denoted as  $\mathbf{X} = (R, \Theta)$  in polar coordinate system, while its new position after deformation is labeled by  $\mathbf{x} = (r, \theta)$ . Then, the geometric deformation gradient tensor  $\mathbf{F} = \partial\mathbf{x} / \partial\mathbf{X}$  can be expressed as the tensor product [47, 50],

$$\mathbf{F} = \mathbf{D} \cdot \mathbf{G}. \quad (3)$$

Here  $\mathbf{G}$  is the growth tensor, which is usually assumed as  $\mathbf{G} = \text{diag}(\gamma_1, \gamma_2)$ , where  $\gamma_1$  is the circumferential growth rate and  $\gamma_2$  is the radial growth rate.  $\mathbf{D}$  is the elastic deformation tensor, the expression of which is  $\mathbf{D} = \text{diag}((\partial r / \partial R) / \gamma_1, (r/R) / \gamma_2)$ . Combining the incremental displacement vector,  $\mathbf{x}(r, \theta) = u(r, \theta)\mathbf{e}_r + v(r, \theta)\mathbf{e}_\theta$ , with the incremental equilibrium tensor equation in Ref. [50], one can compute the deformation at the inner edge of an elastic annulus. An exact analytical solution to the deformation tensor equation is unknown. Nevertheless, non-trivial solutions are found numerically by assuming a sinusoidal solution form [47, 50] as follows:

$$u(r, \theta) = U(r) \text{Cos}[n\theta], \quad v(r, \theta) = V(r) \text{Cos}[n\theta]. \quad (4)$$

Here the integer  $n$  is referred to as the buckling mode, which counts how many buckles are distributed along the inner edge front. Several predictions of this mechanical model are tested by our experimental measurements, which are elaborated on below.

First, according to the buckling model, the number of buckles is expected to increase for a decreasing growth rate under fixed external pressure. In other words, higher buckling modes occur at slower growth. In our experiment, high buckling modes of 18 and above are observed (Fig. 3e, h), consistent with slow growth. Under the experimental conditions of this study, the bacterial growth speed of the annular colony was indeed rather slow. For a close comparison with swarming experiments reported in the literature, we also recorded a bacterial colony originating from a point inoculation along with the annular swarms under the same condition (Fig. S3). The expansion rate of this growing bacterial colony is also much slower compared to the fast growth as reported in [23]. For instance, at 23 hours the surface area of the slow growing point inoculation was only  $0.58 \pm 0.05$  % of the Petri dish area, while a point inoculation under a faster growth condition more consistent with previously published studies covered  $4.12 \pm 0.05$  % of the Petri dish area (Fig. S4).

Second, the theoretical model predicts that, for a fixed growth rate, a small internal pressure only causes low buckling modes, whereas higher buckling modes occur at higher internal pressure. Even though we were unable to measure the internal pressure inside the colony directly, the relative ratio of the pressure on the outer edge ring to the pressure on the inner edge ring can be estimated. The outer edge only showed two big buckles, whereas more than 28 small buckles were observed along the inner edge in one particular experiment (Fig. 1, Fig. 3a, d, g). Since the orientations of rod-shaped bacteria appeared random within a large swarm colony based on microscopic observation (Figure 5 of [52]), the radial and circumferential growth rates within the large annular colony are presumed to be the same, satisfying a criterion known as isotropic growth. The sequential images of the evolving annular colony also recorded the expansion towards both the outer edge and the inner edge. The outer edge has an increasingly larger radius, while the smaller radius of the inner edge becomes even

smaller during the colony expansion. Thus, the density of the outer edge becomes progressively lower than that of the inner edge. Assuming a roughly proportional relationship between the internal pressure and the local bacterial density, the pressure of the inner edge becomes progressively higher than that of the outer edge. This growing disparity accounts for the occurrence of numerous buckles on the inner edge but nearly none at the outer edge.

Third, we observed gradual decrease in the number of buckles over time, as predicted by the buckling instability theory [47, 50]. When counting the buckling modes on the inner edge of the bacterial annulus from 6 to 17 hours after inoculation, we found the number to decrease from around 32 to about 18 (Fig. 3e). Note two small buckles fused into one between 9 and 11.5 hours (Fig. 3a, d, g). The outline of each buckle fits well with an arc (Fig. 3f). The arc height reaches a maximum about 9-11 hours after inoculation. A decrease in the number of buckles is theoretically predicted as the effective thickness of the inner edge ( $t = R_{\text{out}} - R_{\text{in}}$ , as indicated on Fig. 3i) increases. We note, however, that the actual decreases occur one by one, each time as two neighboring buckles merge. This occurs as increasing circumferential stress acts to squeeze the neighboring buckles over time. This post-buckling behavior is also reported in other systems and has been explained by a multilayer buckling model [50]. For the sake of simplicity, however, our analysis has been limited at the one-layer buckling model [47], which makes reasonable predictions on the number of the buckles observed, but not on the post-buckling behavior.

### ***Ring breakup and formation of liquid droplets***

The inner ring of the bacterial annulus undergoes an intriguing, biphasic evolution (Fig. 4). It started with a slow approach towards the center during the first 12 hours, contracting at an average speed of  $-0.15 \mu\text{m/s}$  in radius (Fig. 4b), where the negative sign indicates reducing size. The speed briefly reached  $-0.27 \mu\text{m/s}$  by the 14th hour. Within the next hour, the ring suddenly reversed its contraction and started expansion, briefly at a speed of  $0.56 \mu\text{m/s}$ . This outward, rapid expansion of the ring led to the breakup of the ring into droplets (Fig. 4a). The droplets gradually fused during their outward migration and continuous growth. While the

migration speed of both spherical and sausage-shaped droplets slowed down after 15 hours (Fig. 4b), they kept growing by accreting the incoming bacteria of the outer edge. These droplets then coalesced and fused back into a bolder ring, albeit incomplete (Fig. 4a).

Another interesting observation is a reverse migration of bacteria from the outer edge to the droplets (Fig. 4a and Fig. S1). After 19 hours, the outer ring was depleted. The mechanism of this reverse migration is unknown. One plausible cause may be, since the fluid in the migrating droplets may evaporate faster than the bacterial ring near the outer edge, now the large droplets of active bacteria may induce a reversed capillary flow. This new capillary flow may bring back some bacteria from the outer edge to the outward migrating droplets due to proximity. Further study is required to determine what exact mechanism is responsible for this reverse migration, which only occurred after the inner ring broke up into droplets and while the large droplets migrated outwards.

The decreasing radius of the inner edge concurrent with increasing radius of the outer edge throughout colony expansion (Fig. 3c) may hold the key towards understanding the sudden breakup of the bacterial ring near the inner edge. The slow but persistent expansion of the annular colony must be caused by the flow of cell medium from the agar substrate. Such a flow is osmotically driven by osmolytes produced by the growing bacterial population. During the early stage of growth till hour 14, the bacteria at the inner edge formed a ring of increasing cell density and the ring remained anchored to the inner edge. The sudden breaking of the inner bacterial ring between hour 14 and hour 15 must have occurred as the ring detached from the inner edge. This was inevitable as the ring diameter continued to increase due to growth of the population contained in the ring. In the meantime, cells closer to the inner edge continued to press radially inward, producing the mechanical buckles as observed. Intuitively, this situation can only occur in the condition of slow growth. Otherwise, fast increase in fluid volume would constantly flood the edges and fuel the bacterial spread via contact line expansion, not mechanical buckling.

The breaking up of the inner bacterial ring leads to a return of fluid behavior in terms of the classic Rayleigh–Plateau instability of viscous fluid [53, 54]. Our model hinges upon a key hypothesis that during the rapid expansion at the onset of the inner ring breakup, the densely-packed bacteria within the ring became slightly dispersed upon stress release so that the ring of packed bacteria transformed back into a viscous liquid. The sudden elongation probably caused a periodic perturbation on the surface of bacteria-loaded liquid torus, inducing a circumferential wave on the ring. The local pressure of a viscous liquid column with a perturbation wave on its surface obeys the Young-Laplace law,  $P = \sigma (1/R_c + 1/R_w)$ , where  $\sigma$  represents surface tension,  $R_w$  is the local radius of curvature along the circumferential wave, and  $R_c$  is the cross-sectional radius of the torus (Fig. 4c). The pressure term proportional to  $1/R_c$  tends to push bacteria in the constriction zones to the bulges, whereas the pressure term of circumferential wave proportional to  $1/R_w$  opposes bulging. The two opposite actions are balanced at a critical wavelength [53],  $\lambda_c = 2\pi R_R$ , where  $R_R$  is the initial column radius before the perturbation. When the circumferential wavelength increases above the critical wavelength,  $\lambda > \lambda_c$ , the inner bacterial ring breaks into isolated droplets as shown in Fig. 4a at 15 hr, Fig. S1 at 15 hr, and Fig. S2 at 17 hr.

We now apply the Rayleigh–Plateau instability model in order to account for the droplet size and number observed in our experiments. The number of droplets that occur varies with the annulus size as well as with the thickness of the dense bacterial ring. The wavelength of circumferential wave  $\lambda$  can be estimated by measuring the spacing between periodically distributed droplets along an arc over which the droplets are located. For instance, measuring the spacing between a string of three spherical droplets (the dashed blue curve in Fig. 4a at 16 hr) yields  $\lambda = 0.78 \pm 0.3$  cm. Based on the estimated cross-sectional radius of the ring on the 14 hr image as 1mm, the critical wavelength is estimated as  $\lambda_c = 2\pi R_R = 0.69 \pm 0.5$  cm. These values are crude, but they turn out to be consistent with the prediction  $\lambda > \lambda_c$ . Note the sausage shaped droplets remained unbroken since their cross-sectional radius was bigger than that of the broken arc. The radius of spherical droplets formed after the breaking of a conventional liquid torus is roughly the initial cross-sectional radius  $R_R$  [22]. The total number of spherical

droplets  $n$  is predicted as  $n \approx 0.57 R_{\text{annu}} / R_R$ , where  $R_{\text{annu}}$  is the radius of the center ring of liquid torus. Here our bacterial annulus displays approximately the same linear law. The measured radius of newly generated spherical droplets out of both the bacterial annulus of 3 cm diameter and 7.5 cm diameter are almost the same. Due to variation in growth, periodically distributed spherical droplets only cover short arcs, not continuously over the entire circumference. Nevertheless, we measured the angle covered by a few spherical droplets that formed an arc and deduced the total number of droplets which would cover a complete ring. The estimated numbers are 9 and 28, respectively, for a complete ring of 3 cm and 7.5 cm in diameter (Fig. 1 and Fig. S2). The aspect ratio,  $R_{\text{annu}} / R_R$ , for bacterial annulus of 3 cm and 7.5 cm in diameter are roughly 15 and 37.5, respectively. Thus, we find the linear relationship,  $n \approx c R_{\text{annu}} / R_R$ , to hold, with  $c \approx 0.6 \sim 0.7$ . This value agrees well with the theoretical estimate of 0.57. The agreement confirms that droplet formation from the breaking bacterial ring bears the characteristic of Rayleigh–Plateau instability.

As an additional exercise in applying the droplet instability model, we simulated the velocity flow field and geometric deformation of a short column of viscous fluid under periodic perturbation on surface tension using Comsol-Multiphysics. The results show a flow from the constriction region to the top surface of the bulges, induced by a gradient of surface tension prescribed in the model (Fig. 4d). This predicted flow pattern may be verified by imaging the motion of cells within the droplets. Unfortunately, we have not yet developed the technical capability to do that due to the large size of the droplets formed on top of a thick agar gel.

## Conclusion

A growing bacterial colony is a complex fluid containing densely packed bacteria, and its expansion is governed by both fluid dynamics and elasto-mechanics. The large-scale motility of the bacteria-laden fluid is primarily driven by capillary flow, induced by imbalanced evaporation. The individual motility of the bacteria each propelled by their flagella is not required

to account for the observed colony expansion. Whereas existing theoretical models of biological growth are often complicated, involving multiple parameters and equations [22, 49], we show in this report that each growth stage of an annular bacterial colony is dominated by one mechanical process. For example, the capillary flow and evaporation theory explains the formation of bacterial rings on the edges. The wavelike protrusions at the inner edge can be explained by the buckling model for a hyperelastic solid [47, 50]. After the breakup of the dense bacterial ring, the fragments appear to return to the liquid state due to stress release. The subsequent formation of spherical and sausage-shaped droplets (Fig. 1, Fig. S1, Fig. S2) manifests Rayleigh–Plateau instability [42]. Accretion and droplet coalescence occur in subsequent growth, with characteristic features akin to liquid droplets that form and grow during a liquid-liquid phase separation in other biological systems [55].

We conclude by stating that the physics-based mechanisms elaborated in this report sets the foundation for a broad range of applications involving large scale self-assembly of active matter [56, 57], adhesion [58], biofilm growth [59, 60], infection control [61], etc. In particular, the annular geometry as a template for bacterial growth study may be useful for exploring various properties of both physical and biological origins.

## **Methods**

### **Preparation of bacteria and agar plate**

The bacterium used in this study was *P. aeruginosa* PAO1 (wild type). A sterile metal wire was used to first scrub the surface of a frozen bacterial sample taken out of the  $-80^{\circ}\text{C}$  freezer, and then gently scrub a gel surface containing tryptic soy broth (TSB) with 1.5% agar. After 2 days of growth, we again used a metal wire to take a tiny piece of an expanding bacterial colony and dissolved it into a TSB solution in a 25 ml flask and then incubated the bacterial solution at  $37^{\circ}\text{C}$  with gentle shaking at 100 rpm.

Swarm plates were prepared following the recipe of Xavier *et al.* [62]. To make 250 ml of liquid gel solution, we added 100 ml of 1.25% agar by mass, 93.75 ml water, 50 ml 5X M8 solution (12 g Na<sub>2</sub>HPO<sub>4</sub>, 15 g KH<sub>2</sub>PO<sub>4</sub>, 2.5 g NaCl, dissolved in deionized water to the final volume of 1 L), 250 μL 1M Mg<sub>2</sub>SO<sub>4</sub>, 25μL 1M CaCl<sub>2</sub>, 6.25 ml 200 g/L Casamino Acids (*Bacto*), and 3.125 ml 40% glucose stock solution. Approximately 20 ml of the gel mix in liquid state at above 50 °C was poured into each petri dish. The diameter of the petri dishes used was 9 cm. This size holds for all the plate images, including those shown in the figures and supplemental figures. The petri dishes were placed in the biosafety cabinet for 60 minutes, uncovered, to solidify at room temperature before inoculation. In a control experiment, the agar gel was only allowed 45 min to solidify prior to inoculating, in order to yield faster colony growth and expansion (Figure S4b).

### **Inoculation of bacterial annulus**

A rubber O-ring was dipped into the bacterial solution, which was grown in the flask for 12 hours under the conditions described above, and then gently placed on the surface of the agar gel on a swarm plate for 3-5 sec, forming an invisible bacteria-containing liquid film. The diameters of the rubber O-rings used ranged from 3.0 to 7.5 cm. Although the cross-sectional diameter of the O-ring was less than 2 mm, the cross-sectional width of the annulus stamped with liquid varied, primarily dependent on how much liquid was deposited and how the thin ring of bacteria-laden liquid wetted the agar surface. This annulus width was not precisely controlled, but the value became visibly obvious as the region covered by bacteria became visible hours after inoculation. The colony growth was recorded over 60 hours.

### **Image recording and analysis**

The photos of bacterial colonies were taken using a Cannon7D DSLR camera. Placed on a black bench surface and illuminated by a white light box standing on the side of the plate, the bacterial colonies appeared brighter relative to the agar surface. The intensity profile was extracted by *Image J* and converted into matrix database using *Origin*. We then used the

MatLab 2015 software to produce both pseudo-color 3D and contour plots of intensity alongside with the unprocessed photographs for display purposes.

### Theoretical methods

The flow field distribution on the radial cross section of the bacterial annulus was computed by Comsol-Multiphysics using the CFD module, which is programmed to solve the Navier-Stokes equation,

$$\rho \frac{\partial \mathbf{V}}{\partial t} + \rho(\mathbf{V} \cdot \nabla) \mathbf{V} = \nabla \cdot \left[ -p \mathbf{I} + \eta(\nabla \mathbf{V} + (\nabla \mathbf{V})^T) + \sigma(\mathbf{I} + \mathbf{nn}^T) \delta \right] + \rho \mathbf{g},$$

under the constraint of  $\nabla \cdot \mathbf{V} = \mathbf{0}$ . Here  $\mathbf{V}$  is the velocity of liquid,  $\rho$  is the liquid density,  $P$  is pressure,  $\eta$  is viscosity, and  $\sigma$  is the surface tension. This equation couples to an equation of volume fraction of liquid in air,

$$\rho \frac{\partial \phi}{\partial t} + \mathbf{V} \cdot \nabla \phi = b \nabla \cdot \left[ \varepsilon \nabla \phi - \phi(\mathbf{1} - \phi) \frac{\nabla \phi}{|\nabla \phi|} \right].$$

Here  $\phi$  represents the volume fraction of the liquid in air. The buckling instability for a hyper-elastic tube is simulated by MatLab and Abaqus.

### Acknowledgement

We acknowledge support by the United States National Science Foundation (J.X.T., Grants No. CBET 1438033), and by the China Scholarship Council (T.S.). J.X.T. would like to thank the Isaac Newton Institute for Mathematical Sciences for support and hospitality during the programme entitled Growth, Form, and Self-assembly, when substantial revision of this paper was undertaken (EPSRC grant number EP/K032208/1). We thank co-workers Jordan Bell and Prof. Robert A. Pelcovits for their comments on the manuscript.

### Author Contributions and Information

T.S. and J.X.T. conceived the project, designed the study and wrote the manuscript. Z.M. and J.X.T. performed the experiments. T.S. performed data analysis and theoretical work. The authors declare no competing interests.

## References

1. Ben-Jacob, E., I. Cohen, and H. Levine, *Cooperative Self-Organization of Microorganisms*, Adv. Phys. , 2000. **49**: p. 395.
2. Kearns, D.B., *A Field Guide to Bacterial Swarming Motility*, Nat. Rev. Microbiol., 2010. **8**: p. 634.
3. Be'er, A., R.S. Smith, H. Zhang, E.-L. Florin, S.M. Payne, and H.L. Swinney, *Paenibacillus Dendritiformis Bacterial Colony Growth Depends on Surfactant but Not on Bacterial Motion*, Journal of Bacteriology, 2009. **191**(18): p. 5758-5764.
4. Skerker, J.M. and H.C. Berg, *Direct Observation of Extension and Retraction of Type Iv Pili*, Proceedings of the National Academy of Sciences, 2001. **98**(12): p. 6901-6904.
5. Gibiansky, M.L., J.C. Conrad, F. Jin, V.D. Gordon, D.A. Motto, M.A. Mathewson, W.G. Stopka, D.C. Zelasko, J.D. Shrout, and G.C. Wong, *Bacteria Use Type Iv Pili to Walk Upright and Detach from Surfaces*, Science, 2010. **330**(6001): p. 197-197.
6. Jin, F., J.C. Conrad, M.L. Gibiansky, and G.C. Wong, *Bacteria Use Type-Iv Pili to Slingshot on Surfaces*, Proceedings of the National Academy of Sciences, 2011. **108**(31): p. 12617-12622.
7. Harshey, R.M., *Bacterial Motility on a Surface: Many Ways to a Common Goal*, Annual Reviews in Microbiology, 2003. **57**(1): p. 249-273.
8. Shi, W.Y. and D.R. Zusman, *The Two Motility Systems of Myxococcus Xanthus Show Different Selective Advantages on Various Surfaces*, Proc. Natl. Acad. Sci. USA, 1993. **90**: p. 3378.
9. Thutupalli, S., M. Sun, F. Bunyak, K. Palaniappan, and J.W. Shaevitz, *Directional Reversals Enable Myxococcus Xanthus Cells to Produce Collective One-Dimensional Streams During Fruiting-Body Formation*, Journal of The Royal Society Interface, 2015. **12**(109),
10. Ping, L., Y. Wu, B.G. Hosu, J.X. Tang, and H.C. Berg, *Osmotic Pressure in a Bacterial Swarm*, Biophysical Journal, 2014. **107**(4): p. 871-878.
11. Wu, Y. and H.C. Berg, *Water Reservoir Maintained by Cell Growth Fuels the Spreading of a Bacterial Swarm*, Proceedings of the National Academy of Sciences, 2012. **109**(11): p. 4128-4133.
12. Trinschek, S., K. John, S. Lecuyer, and U. Thiele, *Continuous Versus Arrested Spreading of*

- Biofilms at Solid-Gas Interfaces: The Role of Surface Forces*, Physical Review Letters, 2017. **119**(7): p. 078003.
13. Hennes, M., J. Tailleur, G. Charron, and A. Daerr, *Active Depinning of Bacterial Droplets: The Collective Surfing of Bacillus Subtilis*, Proceedings of the National Academy of Sciences, 2017. p. 201703997.
  14. Seminara, A., T.E. Angelini, J.N. Wilking, H. Vlamakis, S. Ebrahim, R. Kolter, D.A. Weitz, and M.P. Brenner, *Osmotic Spreading of Bacillus Subtilis Biofilms Driven by an Extracellular Matrix*, Proceedings of the National Academy of Sciences, 2012. **109**(4): p. 1116-1121.
  15. Murray, T.S. and B.I. Kazmierczak, *Pseudomonas Aeruginosa Exhibits Sliding Motility in the Absence of Type Iv Pili and Flagella*, J Bacteriol, 2008. **190**(8): p. 2700-2708.
  16. Tuson, H.H. and D.B. Weibel, *Bacteria–Surface Interactions*, Soft Matter, 2013. **9**(17): p. 4368-4380.
  17. Wang, Q., A. Suzuki, S. Mariconda, S. Porwollik, and R.M. Harshey, *Sensing Wetness: A New Role for the Bacterial Flagellum*, The EMBO J., 2005. **24**: p. 2034.
  18. Berdahl, A., C.J. Torney, C.C. Ioannou, J. Faria, and I.D. Couzin, *Emergent Sensing of Complex Environments by Mobile Animal Groups*, Science, 2013. **339**: p. 574.
  19. Davies, D.G., M.R. Parsek, J.P. Pearson, B.H. Iglewski, J.W. Costerton, and E.P. Greenberg, *The Involvement of Cell-to-Cell Signals in the Development of a Bacterial Biofilm*, Science, 1998. **280**: p. 295.
  20. Mimura, M., H. Sakaguchi, and M. Matsushita, *Reaction Diffusion Modelling of Bacterial Colony Patterns*, Physica A, 2000. **282**: p. 283.
  21. Giverso, C., M. Verani, and P. Ciarletta, *Branching Instability in Expanding Bacterial Colonies*, Journal of the Royal Society, Interface / the Royal Society, 2015. **12**(104): p. 20141290.
  22. Giverso, C., M. Verani, and P. Ciarletta, *Emerging Morphologies in Round Bacterial Colonies Comparing Volumetric Versus Chemotactic Expansion*, Biomech. Model. Mechanobiol., 2016. **15**: p. 643.
  23. Fauvart, M., P. Phillips, D. Bachaspatimayum, N. Verstraeten, J. Fransaer, J. Michiels, and J. Vermant, *Surface Tension Gradient Control of Bacterial Swarming in Colonies of Pseudomonas Aeruginosa*, Soft Matter, 2012. **8**: p. 70.
  24. Yang, A., W.S. Tang, T. Si, and J.X. Tang, *Influence of Physical Effects on the Swarming Motility*

- of Pseudomonas Aeruginosa*, Biophysical Journal, 2017. **112**(7): p. 1462-1471.
25. Ke, W.-J., Y.-H. Hsueh, Y.-C. Cheng, C.-C. Wu, and S.-T. Liu, *Water Surface Tension Modulates the Swarming Mechanics of Bacillus Subtilis*, Frontiers in microbiology, 2015. **6**: p. 1017.
  26. Köhler, T., L.K. Curty, F. Barja, C. Van Delden, and J.-C. Pechère, *Swarming of Pseudomonas Aeruginosa Is Dependent on Cell-to-Cell Signaling and Requires Flagella and Pili*, Journal of Bacteriology, 2000. **182**(21): p. 5990-5996.
  27. Toutain, C.M., M.E. Zegans, and G.A. O'Toole, *Evidence for Two Flagellar Stators and Their Role in the Motility of Pseudomonas Aeruginosa*, Journal of Bacteriology, 2005. **187**(2): p. 771-777.
  28. Kuchma, S., A. Ballok, J. Merritt, J. Hammond, W. Lu, J. Rabinowitz, and G.A. O'Toole, *Cyclic-Di-Gmp-Mediated Repression of Swarming Motility by Pseudomonas Aeruginosa: The Pily1 Gene and Its Impact on Surface-Associated Behaviors*, Journal of Bacteriology, 2010. **192**(12): p. 2950-2964.
  29. Anyan, M.E., A. Amiri, C.W. Harvey, G. Tierra, N. Morales-Soto, C.M. Driscoll, M.S. Alber, and J.D. Shroff, *Type Iv Pili Interactions Promote Intercellular Association and Moderate Swarming of Pseudomonas Aeruginosa*, Proceedings of the National Academy of Sciences, 2014. **111**(50): p. 18013-18018.
  30. Soberón-Chávez, G., F. Lépine, and E. Déziel, *Production of Rhamnolipids by Pseudomonas Aeruginosa*, Applied Microbiology and Biotechnology, 2005. **68**(6): p. 718-725.
  31. Caiazza, N.C., R.M. Shanks, and G. O'Toole, *Rhamnolipids Modulate Swarming Motility Patterns of Pseudomonas Aeruginosa*, Journal of Bacteriology, 2005. **187**(21): p. 7351-7361.
  32. Tremblay, J., A.P. Richardson, F. Lépine, and E. Déziel, *Self-Produced Extracellular Stimuli Modulate the Pseudomonas Aeruginosa Swarming Motility Behaviour*, Environmental microbiology, 2007. **9**(10): p. 2622-2630.
  33. Tremblay, J. and E. Déziel, *Improving the Reproducibility of Pseudomonas Aeruginosa Swarming Motility Assays*, Journal of basic microbiology, 2008. **48**(6): p. 509-515.
  34. Doyle, T.B., A.C. Hawkins, and L.L. McCarter, *The Complex Flagellar Torque Generator of Pseudomonas Aeruginosa*, Journal of bacteriology, 2004. **186**(19): p. 6341-6350.
  35. O'toole, G.A. and R. Kolter, *Flagellar and Twitching Motility Are Necessary for Pseudomonas Aeruginosa Biofilm Development*, Molecular microbiology, 1998. **30**(2): p. 295-304.

36. Lieleg, O., M. Caldara, R. Baumgärtel, and K. Ribbeck, *Mechanical Robustness of Pseudomonas Aeruginosa Biofilms*, *Soft Matter*, 2011. **7**(7): p. 3307-3314.
37. Overhage, J., M. Bains, M.D. Brazas, and R.E. Hancock, *Swarming of Pseudomonas Aeruginosa Is a Complex Adaptation Leading to Increased Production of Virulence Factors and Antibiotic Resistance*, *Journal of bacteriology*, 2008. **190**(8): p. 2671-2679.
38. Ristenpart, W.D., P.G. Kim, C. Domingues, J. Wan, and H.A. Stone, *Influence of Substrate Conductivity on Circulation Reversal in Evaporating Drops*, *Phys. Rev. Lett.*, 2007. **99**: p. 234502.
39. Shereshefsky, J.L. and S. Steckler, *A Study of the Evaporation of Small Drops and of the Relationship between Surface Tension and Curvature* *J. Chem. Phys.* , 1936. **4**: p. 108.
40. Deegan, R.D., O. Bakajin, T.F. Dupont, G. Huber, S.R. Nagel, and T.A. Witten, *Capillary Flow as the Cause of Ring Stains from Dried Liquid Drops*, *Nature*, 1997. **389**: p. 827.
41. Kooij, H.M.v.d., G.T.v.d. Kerkhofa, and J. Sprakel, *A Mechanistic View of Drying Suspension Droplets*, *Soft Matter*, 2016. **12**: p. 2858.
42. Pairam, E. and A. Fernandez-Nieves, *Generation and Stability of Toroidal Droplets in a Viscous Liquid*, *Phys. Rev. Lett.*, 2009. **102**: p. 234501.
43. Banaha, M., A. Daerr, and L. Limat, *Spreading of Liquid Drops on Agar Gels*, *The European Physical Journal-Special Topics*, 2009. **166**(1): p. 185-188.
44. Brochard-Wyart, F. and P. De Gennes, *Dynamics of Partial Wetting*, *Advances in colloid and interface science*, 1992. **39**: p. 1-11.
45. De Gennes, P.-G., *Wetting: Statics and Dynamics*, *Reviews of modern physics*, 1985. **57**(3): p. 827.
46. Delarue, M., J. Hartung, C. Schreck, P. Gniewek, L. Hu, S. Herminghaus, and O. Hallatschek, *Self-Driven Jamming in Growing Microbial Populations*, *Nature physics*, 2016.
47. Moulton, D.E. and A. Goriely, *Circumferential Buckling Instability of a Growing Cylindrical Tube*, *J. Mech. Phys. Solids*, 2011. **59**: p. 525.
48. Lee, M.M.L. and S. Chien, *Morphologic Effects of Pressure Changes on Canine Carotid Artery Endothelium as Observed by Scanning Electron Microscopy*, *Anat. Rec.* , 1978. **194**: p. 1.
49. Maclaurin, J., J. Chapman, G.W. Jones, and T. Roose, *The Buckling of Capillaries in Solid Tumours*, *Proc. R. Soc. A*, 2012. **468**: p. 4123.

50. Li, B., Y.P. Cao, X.Q. Feng, and H. Gao, *Surface Wrinkling of Mucosa Induced by Volumetric Growth: Theory, Simulation and Experiment.*, J. Mech. Phys. Solids, 2011. **59**: p. 758.
51. De Dier, R., W. Sempels, J. Hofkens, and J. Vermant, *Thermocapillary Fingering in Surfactant-Laden Water Droplets*, Langmuir, 2014. **30**(44): p. 13338-13344.
52. Du, H., Z. Xu, M. Anyan, O. Kim, W.M. Leevy, J.D. Shrout, and M. Alber, *High Density Waves of the Bacterium Pseudomonas Aeruginosa in Propagating Swarms Result in Efficient Colonization of Surfaces*, Biophysical Journal, 2012. **103**(3): p. 601-609.
53. Rayleigh, S.R.S.L., *On the Instability of a Cylinder of Viscous Liquid under Capillary Force*, Phil. Mag. S. 5, 1892. **34**: p. 145.
54. Eggers, J., *Nonlinear Dynamics and Breakup of Free-Surface Flows*, Rev. Mod. Phys., 1997. **69**: p. 865.
55. Hyman, A.A., C.A. Weber, and F. Jülicher, *Liquid-Liquid Phase Separation in Biology*, Annual review of cell and developmental biology, 2014. **30**: p. 39-58.
56. Koch, D.L. and G. Subramanian, *Collective Hydrodynamics of Swimming Microorganisms: Living Fluids*, Annu. Rev. Fluid. Mech., 2010. **43**(1): p. 637.
57. Ramaswamy, S., *The Mechanics and Statistics of Active Matter*, Annu. Rev. Cond. Mat. Phys., 2010. **1**: p. 323-345.
58. Morra, M. and C. Cassinelli, *Bacterial Adhesion to Polymer Surfaces: A Critical Review of Surface Thermodynamic Approaches*, Journal of Biomaterials Science-Polymer Edition, 1997. **9**(1): p. 55-74.
59. Morikawa, M., *Beneficial Biofilm Formation by Industrial Bacteria Bacillus Subtilis and Related Species*, J. Biosci. Bioeng., 2006. **101**: p. 1.
60. Tan, S.Y.-E., S.C. Chew, S.Y.-Y. Tan, M. Givskov, and L. Yang, *Emerging Frontiers in Detection and Control of Bacterial Biofilms*, Current opinion in biotechnology, 2014. **26**: p. 1-6.
61. Diggle, S.P., A.S. Griffin, G.S. Campbell, and S.A. West, *Cooperation and Conflict in Quorum-Sensing Bacterial Populations*, Nature, 2007. **450**: p. 411.
62. Xavier, J.B., W. Kim, and K.R. Foster, *A Molecular Mechanism That Stabilizes Cooperative Secretions in Pseudomonas Aeruginosa*, Mol. Microbiol., 2011. **79**: p. 166.

## Figures and Captions

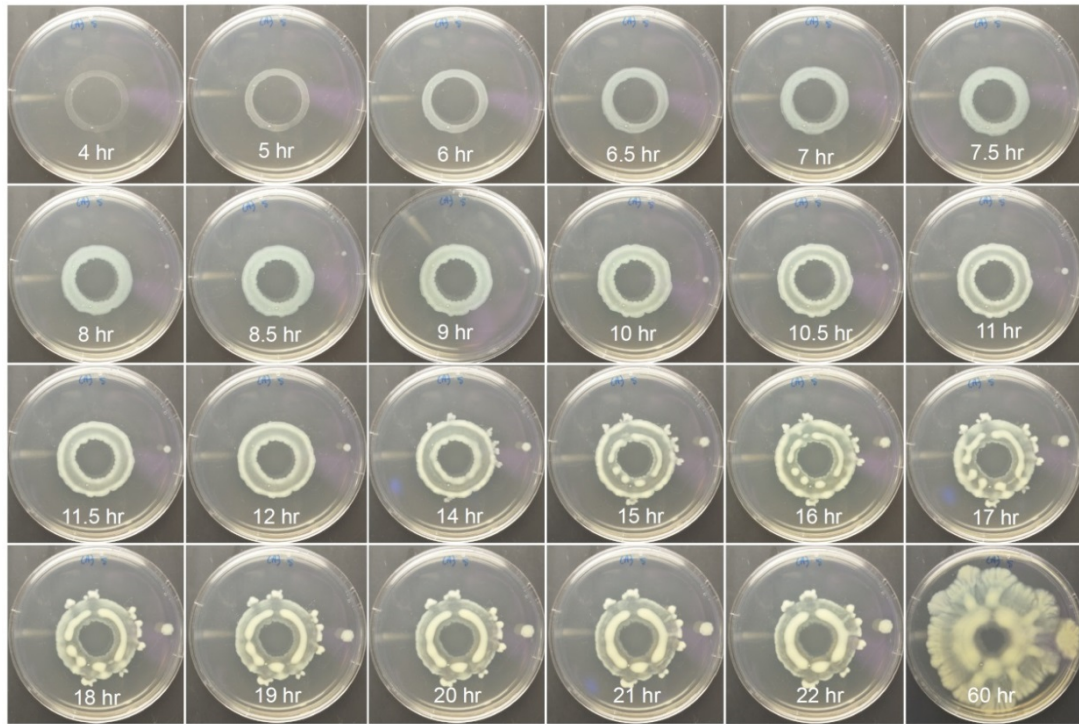


**Figure 1.** The pattern evolution of an annular *P. aeruginosa* colony. The bright white annular region is dense in bacteria. The bacteria grew homogeneously over the first 4 hours. From 5-10 hours, both inner and outer edges grew thicker and denser in bacteria. Periodic protrusions occurred at the front of the inner ring. By 14-15 hours, the dense ring of bacteria at the inner edge broke into isolated droplets. These droplets migrated outwards as they continued to grow. After 19 hours, most droplets had merged to form one bolder ring near the centerline, with additional bacteria recruited from the outer ring. The petri plate diameter is 9 cm.

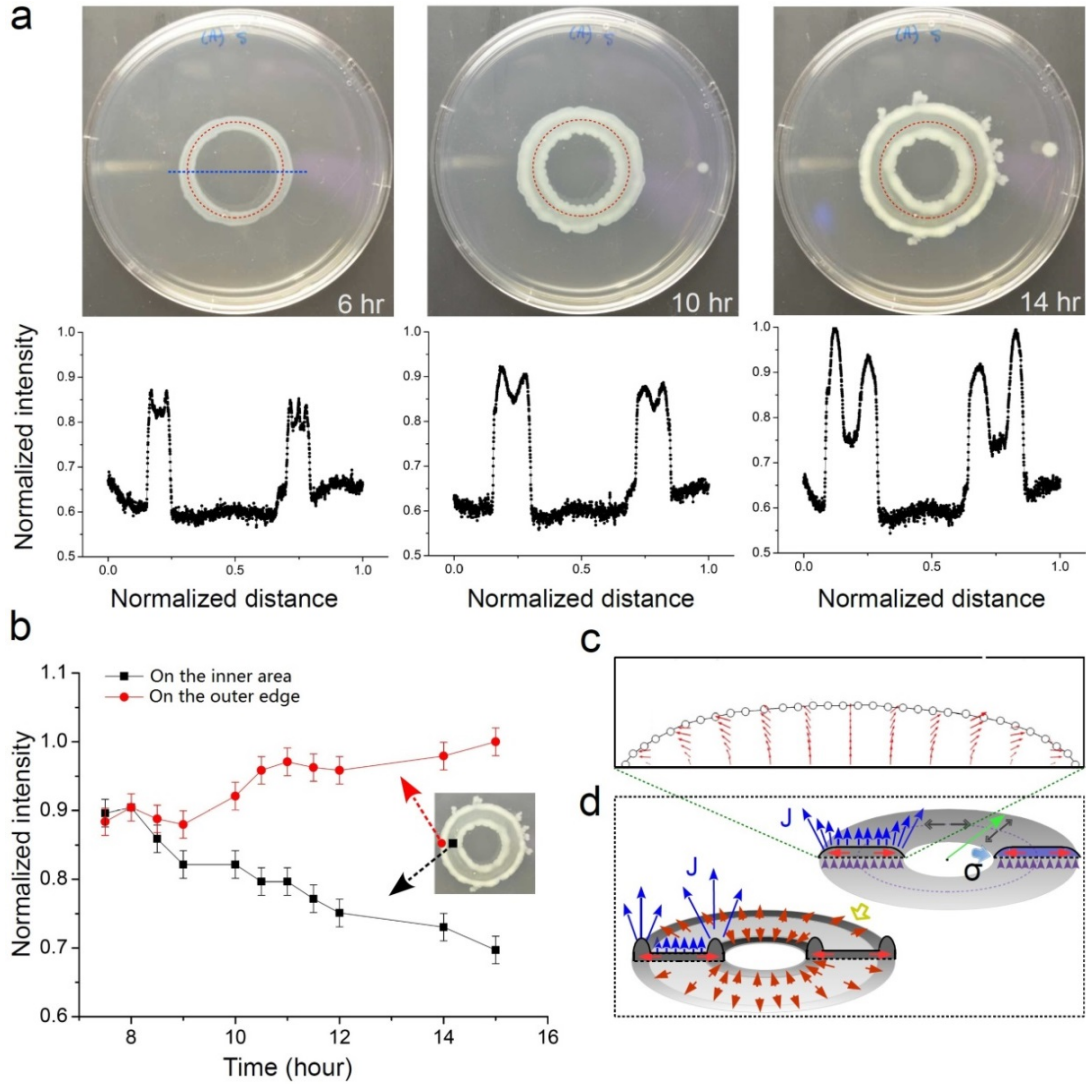


**Figure 2. Analysis of bacterial accumulation on both inner and outer edges.** (a) Magnified view of three photos in Fig. 1, taken 6, 10, and 14 hours after inoculation. These images show the key process of bacteria flowing to edges. The dashed red circle indicates the center-line of the initially stamped annulus. Below each image is a measured intensity profile, normalized to the maximal brightness, along a line passing through the center of the annulus (the dashed blue line in the 6-hour photo). The distance is normalized to the length of the blue line, with value 1 representing 5.16 cm. (b) Measured intensity at a point on the outer edge (red dot) and one on the inner area (black square). The density of bacteria on the outer edge increases with time, while that on the inner area decreases. (c) Cross-sectional view of computed flow field (red arrows) inside the annular bacterial swarm. The parameters chosen for the simulation include the liquid density  $\rho = 1000 \text{ kg/m}^3$ , the dynamic viscosity  $\eta = 0.001 \text{ Pa}\cdot\text{s}$ , and average velocity of fluid out of the bottom surface  $v = 1.0 \text{ }\mu\text{m/s}$ . The outflow speed

on the top boundary is set by an evaporation flux equation,  $J(x) * 2.0 \mu\text{m/s}$  (see text). (d) Schematics showing the capillary flow induced by a notable difference in evaporation flux between the edges and the inner area. The blue arrows indicate the evaporation flux,  $J$ . The red arrows indicate the bacterial migration carried by the capillary flow.

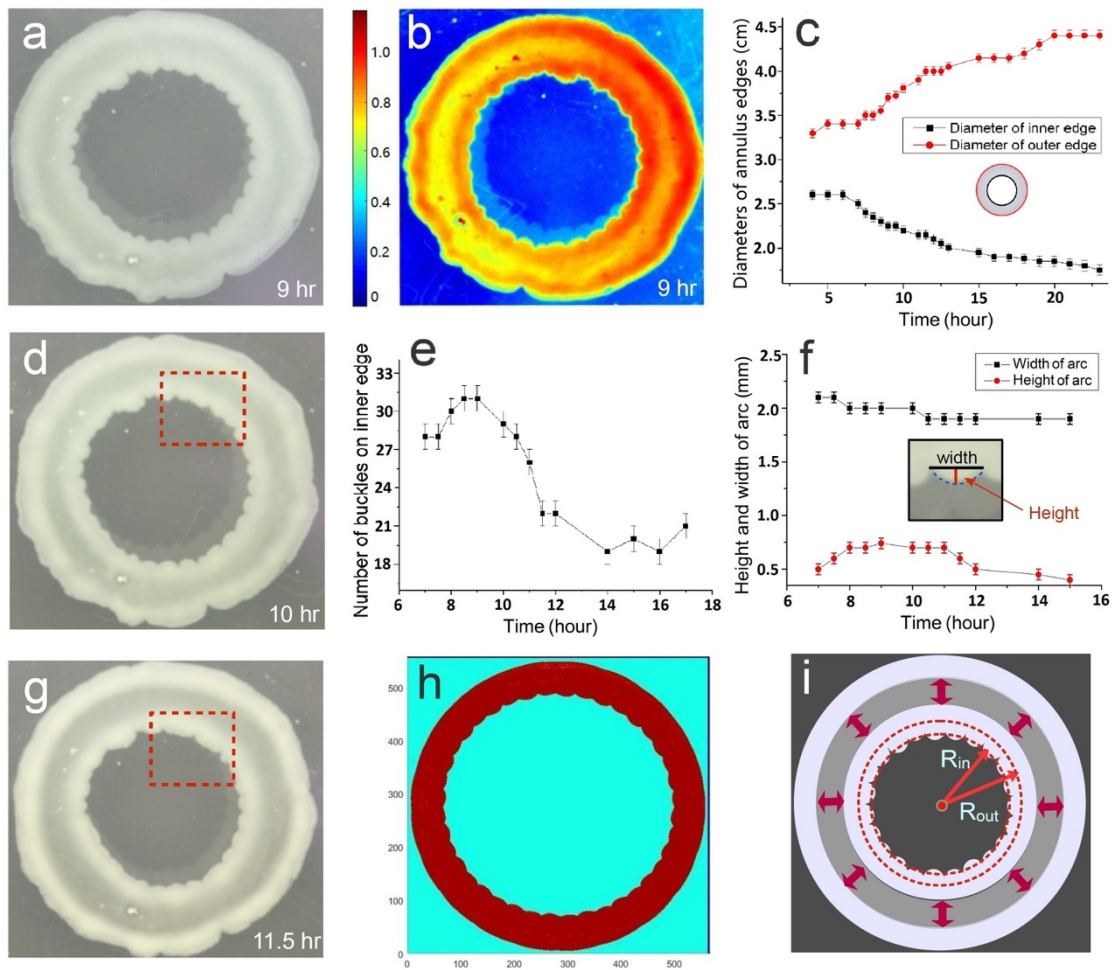


**Figure 3. Buckling instability at the inner swarm front.** (a) The bacterial swarm developed wavelike protrusions at the inner edge 9 hours after inoculation. (b) Contour plot of the bacterial intensity, with values shown in false color. Note a clear density difference between on the edges and at the inner area. (c) The measured inner diameter and outer diameter of the bacterial annulus with initial centerline diameter of 3 cm. The inner diameter decreased while the outer diameter increased over time. The increase in cross-sectional width of the annulus was due to continuous growth and expansion of the bacterial population. (d, g) Images over subsequent hours showing post-buckling pattern progression. The dotted red box indicates two small buckles fusing into one. (e) The number of buckles measured from 7 hours to 18 hours after inoculation. (f) The height and width of a typical buckle arc measured during the same period of time. (h) Theoretical prediction of the buckled configuration on the cross-section of a growing elastic tube based on the one-layer buckling model [47]. For simplicity, the circumferential growth rate  $\gamma_1$  and radial growth rate  $\gamma_2$  are set to be equal,  $\gamma_1 = \gamma_2 = \gamma$ . For a

fixed thickness parameter,  $R_{in}/R_{out} = 0.93$ , when the growth rate parameter  $\gamma$  decreases from 2 to 1.3, the total number of buckles increases from 7 to 32 [47]. (i) A schematic graph depicting how the buckling model is geometrically applied to the bacterial annulus.  $R_{in}$  and  $R_{out}$  are the inner radius and the outer radius of the hyper-elastic inner edge (the annular zone between the two dashed red circles), respectively.

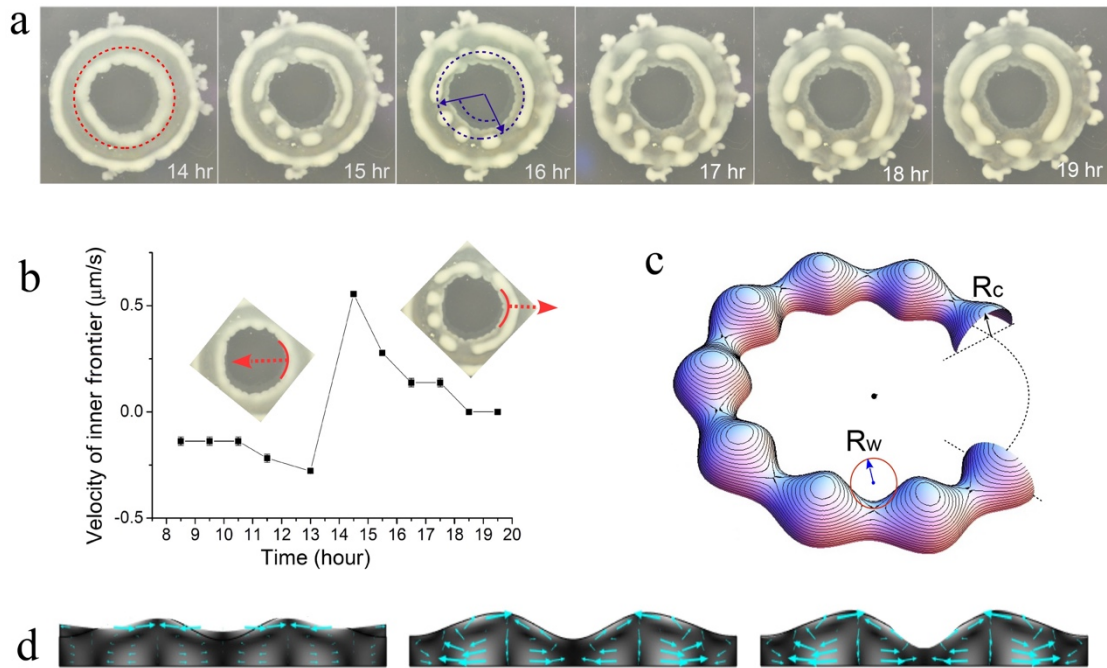


**Figure 4. Droplet occurrence caused by Rayleigh-Plateau instability and subsequent coalescence due to droplet growth.** (a) Sequential images from 14 to 19 hours, showing a sudden expansion of the inner edge ring, its breaking into droplets, and the fusion of these droplets. (b) The average radial velocity of the migrating inner edge measured 8-20 hours after inoculation. The red arrow indicates the migration direction of the inner ring. (c) Geometric illustration of a perturbed torus. The radius  $R_c$ , which varies periodically along the centerline of the torus, measures the boldness of the liquid column.  $R_w$  is the radius of curvature along the wavy surface of the torus. (d) Theoretical prediction of a viscous liquid column breaking into droplets under a perturbation on surface tension. The top half of the cross-section of a cylindrical water column is shown, as it lays horizontally. The three images illustrate the time progression of the fluid surface (top contour), with arrows (cyan) indicating the local flow velocity and direction. The chosen parameters for the simulation include: the density of liquid  $\rho = 1000 \text{ Kg/m}^3$ , the dynamic viscosity  $\eta = 0.0015 \text{ Pa.S}$ , and the reference surface tension  $\sigma_0 = 0.06 \text{ N/m}$ . The perturbed surface tension is  $\sigma = \sigma_0(1 - 0.2\cos(kx)) \text{ N/m}$ , with the wave number  $k = 5\pi/60$ . Droplet formation as shown here occurs over a wide range of viscosity and density. However, it sensitively depends on the wave number of the perturbation.

## Supplemental Figures

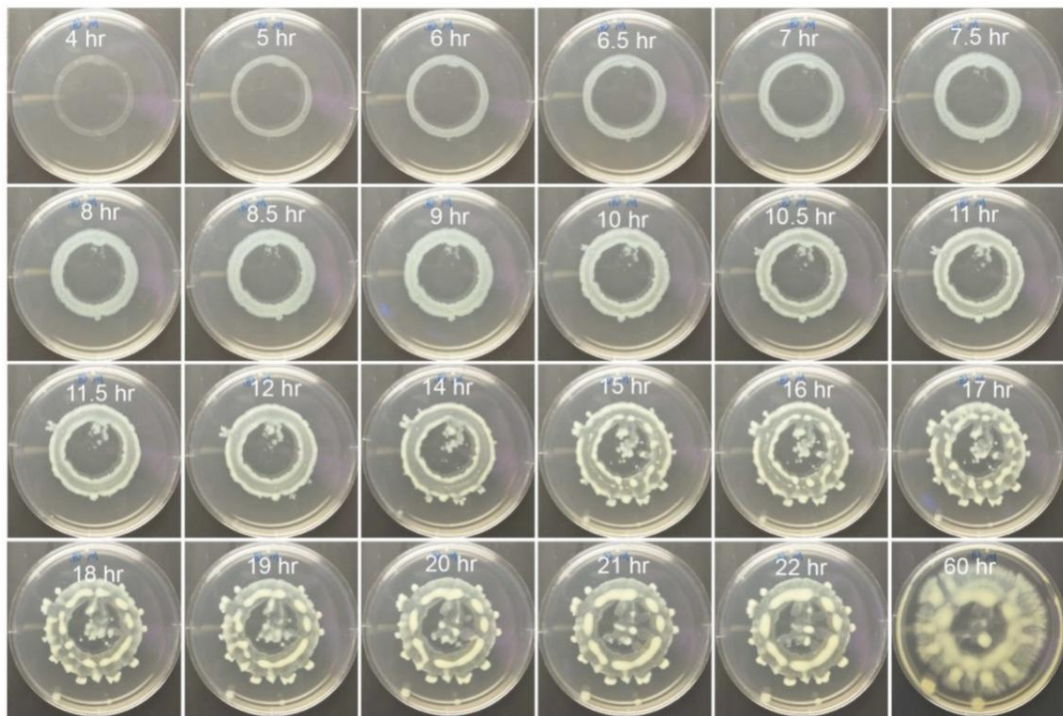


**Figure. S1.** The pattern evolution of a bacterial colony inoculated as a 4 cm diameter lus. Note regularly distributed buckles along the inner edge 9-12 hours after the inoculation. The inward migrating inner ring suddenly reversed its movement to expand outwards within the 14-15 hour window. At the same time, the continuous arc broke into isolated droplets. The diameter of the petri dish is 9 cm, as it holds for subsequent figures.

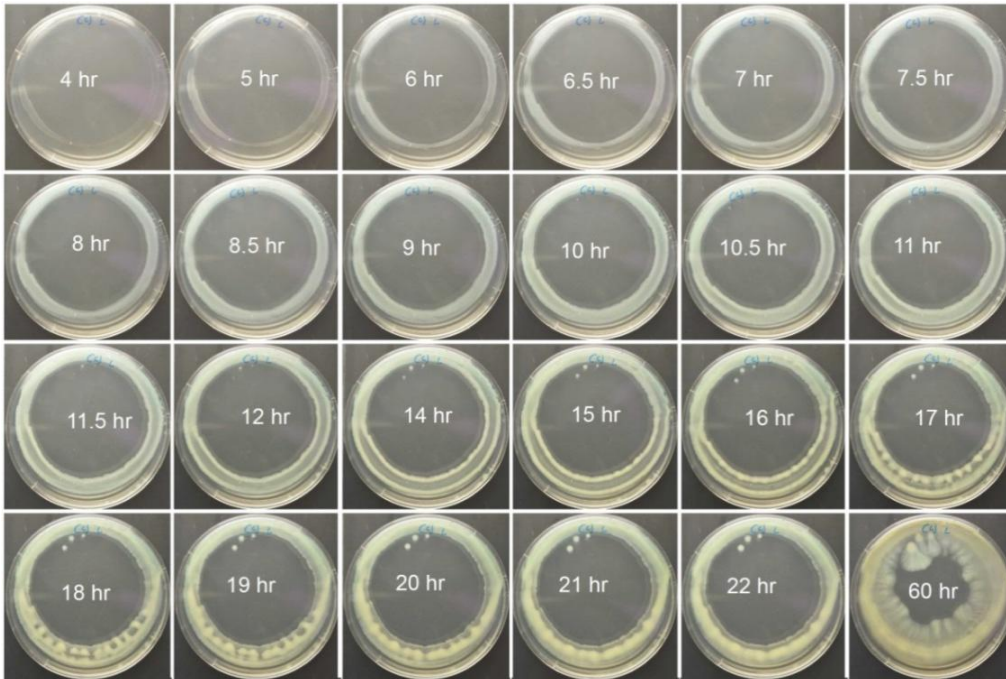


**Figure. S2.** The pattern evolution of a bacterial colony inoculated as a 7.5 cm diameter annulus. Regularly distributed droplets occurred along the inner edge by 17 of growth. Small fingerlike protrusions grew out of the inner edge in the later swelling process after 22 hours.

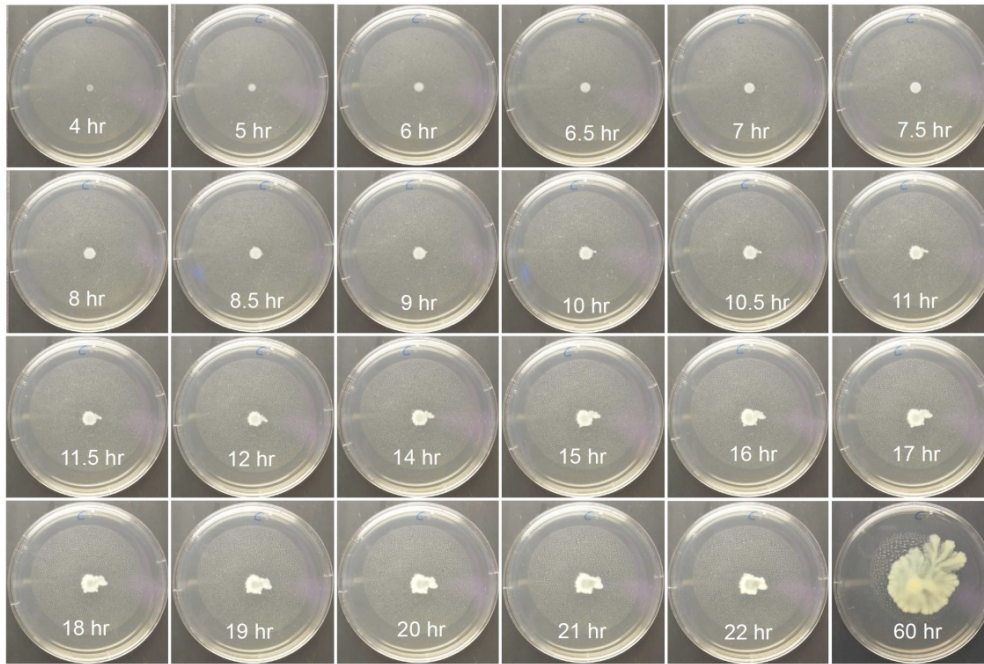


**Figure S3.** The pattern evolution of a *P. aeruginosa* colony inoculated as a point source at the center of the plate. Note a layer of tiny water droplets condensed on the cover. The growth rate of this bacteria colony is rather slow compared with other published experiments on bacterial swarming out of point inoculation [23, 24]. The annular colony growth experiments in this report were performed at a slow growth condition.

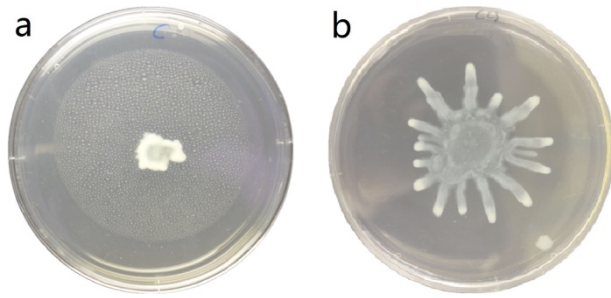


**Figure S4.** A slow-expanding colony and a faster-expanding colony, both originated at a point at the plate center. (a) A slowly growing bacterial colony photographed at 23 h. This plate was prepared under the same condition as for the annular swarm observation. Note a layer of water droplets condensed on the cover. (b) A faster-growing bacterial colony photographed at 23 hours in another experiment, with shorter time of drying to allow for agar gelation prior to inoculation (45 min vs 60 min).